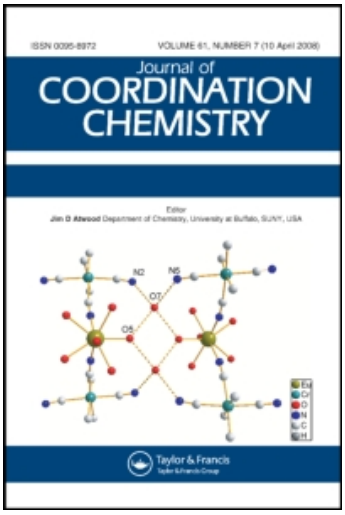


**Journal of Coordination Chemistry**
Publication details, including instructions for authors and subscription information:
http://www.informaworld.com/smpp/title~content=t713455674

# Supramolecular modeling in novel polymeric complexes of ruthenium and uranium derived from azoquinoline containing hydrogen bonds

Ahmed T. Mubarak[a]
[a] Faculty of Science, Department of Chemistry, King Khalid University, Abha 61413, Saudi Arabia

**To cite this Article** Mubarak, Ahmed T.(2007) 'Supramolecular modeling in novel polymeric complexes of ruthenium and uranium derived from azoquinoline containing hydrogen bonds', Journal of Coordination Chemistry, 60: 16, 1731 — 1747
**To link to this Article: DOI:** 10.1080/00958970601117381
**URL:** http://dx.doi.org/10.1080/00958970601117381

*Journal of Coordination Chemistry*
Vol. 60, No. 16, 15 August 2007, 1731–1747

Taylor & Francis
Taylor & Francis Group

# Supramolecular modeling in novel polymeric complexes of ruthenium and uranium derived from azoquinoline containing hydrogen bonds

AHMED T. MUBARAK*

Faculty of Science, Department of Chemistry, King Khalid University,
P.O. Box 9004, Abha 61413, Saudi Arabia

(*Received 28 November 2006; in final form 3 March 2006*)



Novel polymeric complexes of $Ru^{3+}$ and $UO_2^{2+}$ with 5-(2$^-$-alkyl phenylazo)-8-quinolinol ($LnH_2$) have been prepared and characterized by elemental and thermogravimetric analysis (TGA), $^1H$ and $^{13}C$ NMR, magnetic susceptibility and electronic spectral techniques. The important infrared (IR) bands and the main $^1H$ and $^{13}C$ NMR signals are assigned and discussed relative to the proposed molecular structure of the polymeric complexes. The spectra show that all complexes are octahedral with chloride attached to the metal. The spectral data were utilized to compute the important ligand field parameters B, $\beta$ and Dq. The B-values suggest covalency in the metal-ligand $\sigma$-bond and the Dq-values indicate a medium strong ligand field. $\beta$ depends greatly on the electronegativity of the donor atoms and the ligand structure and also the effect of the *o*-substituent groups. The ligands are dibasic (bis-bidentate chelating agent), coordinating through CN, N=N, COOH, OH and SH groups by replacement of a proton from the last three groups. The bond lengths and the force constants of the U–O bond were calculated from the IR data related to the electronic properties of the substituents. Considerable interest has been focused on the synthesis of azo compounds and polymeric metal complexes. The stability of these complexes has also been investigated. *O*-azo-quinolinols intramolecular OH–N hydrogen bonds have been detected and discussed.

*Keywords*: Supramolecular structures; Hydrogen-bonding; Polymeric complexes; Dimer; Racah parameters

## 1. Introduction

Azo compounds receive attention due to their use as models for biological systems [1, 2]. The driving force for investigating and developing an understanding into the coordinaton behavior and chemical equilibria of these novel compounds has been based on the importance of studying metal-ligand affinities, stereochemistry and substitution properties of the complexes involved [3–6]. Efforts have been made to carry out detailed studies to synthesize and elucidate the structural and electronic properties of new families of complexes with quinoline derivatives as chelating bis-bidentate azodye models.

*Email: atmubarak@kku.edu.sa


ISSN 0095-8972 print/ISSN 1029-0389 online 
DOI: 10.1080/00958970601117381

*O*-alkylazo-8-quinolinols ($LnH_2$) and their related compounds (scheme 1B) have been extensively used as ligands in transition metal coordination chemistry [3–6]. Ease of synthesis, favorable steric arrangement and variability of donor sites that these ligands possess with suitable constituents, make these ligands excellent candidates for constructing new families of complexes of interest.

Although, no structural chemistry or coordination studies have been reported on ligands containing both azo and quinoline groups, data from our laboratory [3–6] have demonstrated that the bis-bidentate azodyes ligands play a key role in making new polymeric complexes with transition metal ions. However, little is known concerning

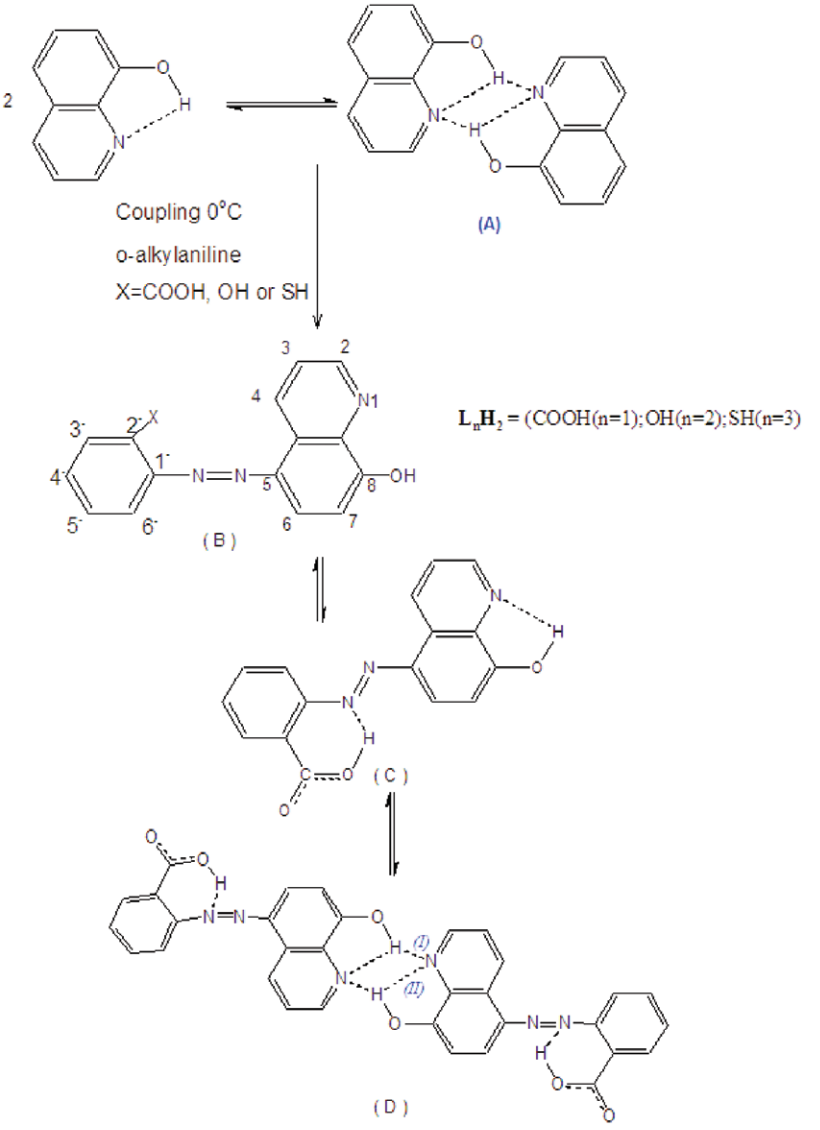


Scheme 1. Representative structure of dimer in the solid state.

the constitution of these complexes, the chemistry involved in their preparation, or the structures and coordination in such complexes.

It has been shown from IR spectral data [2–5] that hydrogen bonding plays an important role in biological systems. Due to the higher number of hydrogen bonds, the Watson–Crick pair of guanine and cytosine is more stable than the thymine-adenine complex [7]. Moreover, Jørgensen found [8] that the stability of multiple hydrogen bonded "dimers" depends not only on the number of hydrogen bonds but also on the hydrogen bonding pattern.

The importance of clarifying the structure and stability of hydrogen-bonded complexes has opened up an area of surface science that has attracted considerable attention in environmental chemistry.

In this article, we investigate the metal coordination of azo 8-hydroxyquinoline derivatives as well as the hydrogen bonding of these molecules. We report studies of: (i) the synthesis of new substituted phenylazo-8-quinoline ($LnH_2$) ligands, (ii) the synthesis of $Ru^{3+}$ and $UO_2^{2+}$ complexes derived from these ligands, (iii) investigations of the stereochemistry of the complexes based on the electronic spectra and other measurements, (iv) determining the vibrational mode of bonding, stability and structures of the hydrogen-bonding in the novel polymeric complexes.

In addition, we will discuss previous studies of hydrogen bonding [9] and compare them with the results of the present investigation in order to provide a better explanation of the chemical behavior of such complexes, allowing the reversible formation of aggregates which are not covalently linked.

Work is underway in studying the dimerization behavior of azo 8-hydroxyquinoline and its derivatives in the presence of some metal ions in order to gain a better insight into the chemistry of the formed supramolecular materials.



## 2. Experimental

Standard chemicals 8-hydroxyquinoline and 2-derivatives aniline were used without any further purification; $RuCl_3 \cdot 3H_2O$ and $UO_2(CH_3COO)_2 \cdot 3H_2O$ (Aldrich) were used as supplied.

### 2.1. *Preparation of the ligands*

5-($2^-$-alkylphenylazo)-8-quinolinols ($LnH_2$) were typically prepared by adding 25 mL of distilled water containing hydrochloric acid (12 M, 2.68 mL, 32.19 mmol) to 2-alkylphenylazo-8-quinolinols ($LnH_2$) (10.73 mmol). To the resulting mixture, stirred and cooled to 0°C, a solution of sodium nitrite (740 mg, 10.73 mmol, in 20 mL of water) was added dropwise. The formed diazonium chloride was coupled with an alkaline solution of 8-hydroxyquinoline (1.56 g, 10.73 mmol) in 20 mL of ethanol containing 602 mg (10.73 mmol) of potassium hydroxide. The orange precipitate, which formed immediately was filtered and washed several times with water. The crude product obtained was purified by crystallization from hot ethanol. Elemental anal. calcd. were as follows: $C_{16}H_{11}N_3O_3(L_1H_2)$ yield (~68%): C, 65.5; H, 3.8; N, 14.3. found: C, 65.4; H, 3.8; N, 14.6%, $C_{15}H_{11}N_3O_2$ ($L_2H_2$) yield (~77%): C, 67.9; H, 4.2; N, 15.9; found: C,

67.8; H, 4.2; N, 16.2% and $C_{15}H_{11}N_3OS(L_3H_2)$ yield (~60%): C, 64.1; H, 3.9; N, 15.0; found: C, 64.0; H, 4.1; N, 15.3%.

### 2.2. *Preparation of the complexes*

The metal chelates were isolated by reacting ethanolic solutions of the metal chloride and/or acetate and the ligands in stoichiometric proportion with stirring at room temperature and then maintained at reflux temperature on a water bath for 1.5 h. The products were filtered, washed with EtOH, $Et_2O$ and dried in vacuo at 40°C for several days when the polymeric complexes were collected as powders.

## 3. Measurements



Microanalyses of all samples were carried out at King Khalid University Analytical Center, Saudi Arabia, using a Perkin-Elmer 2400 Series II Analyzer. The metal content in the polymeric complexes was estimated by standard methods [3–6]. IR spectra were recorded on a Perkin-Elmer 1340 spectrophotometer. UV-Vis spectra were measured (Nujol mull) on a Pye Unicam 8800 spectrophotometer. Magnetic measurements were carried out at room temperature using Gouy's method, employing $Hg[Co(SCN)_4]$ for calibration, and were corrected for diamagnetism by using Pascal's constant. Magnetic moments were calculated using the equation: $\mu_{eff} = 2.84\ [T\chi_M^{corr}]^{1/2}$.

$^1H$ and $^{13}C$ NMR spectra were obtained on a JEOL FX900 Q Fourier transform spectrometer with DMSO–$d_6$ as solvent and TMS as internal reference. TG measurements were made using a DuPont 950 thermo balance. Ten milligram samples were heated at $10^\circ\,min^{-1}$ in a dynamic nitrogen atmosphere ($70\,ml\,min^{-1}$) in a boat-shaped sample holder, $10 \times 5 \times 2.5$ mm deep; the temperature-measuring thermocouple was placed within 1 mm of the holder. The halogen content was determined by combustion of the solid complex (30 mg) in an oxygen flask in the presence of a KOH–$H_2O_2$ mixture. The halide content was then determined by titration with a standard $Hg(NO_3)_2$ solution using diphenyl carbazone as indicator.

The purity of the desired products depends, to a great extent, on the particular reaction employed. For example, reaction of $LnH_2$ with metal chloride gives a low yield even on prolonged refluxing; whereas, reaction with metal acetate is found to be most satisfactory. The yields were varied between ~55 to 85%, depending on the ligand as seen in table 1.

## 4. Results and discussion

The low molar conductance values of all the complexes indicated their non-electrolytic character. All complexes were stable at room temperature and non-hygroscopic in nature, decomposing on heating at >300°C and almost insoluble in water. The complexes are not soluble in common organic solvents, but soluble in DMF and DMSO. The 1 : 1 stoichiometry of the complexes has been concluded from their

Table 1. Analytical data of isolated uranyl and ruthenium complexes (for molecular structures, see schemes 1 and 2).

| | Found (Calcd)% | | | | | | |
|---|---|---|---|---|---|---|---|
| Complex* | C | H | N | Cl[b] | Metal | Composition[a] | Yield (%) |
| **1** | 32.0(32.1) | 1.6(1.7) | 7.2(7.0) | – | 39.9(40.3) | $[UO_2L_1 \cdot 2H_2O]_n$ | 75 |
| **2** | 31.7(31.6) | 1.8(1.8) | 7.7(7.4) | – | 41.8(41.5) | $[UO_2L_2 \cdot 2H_2O]_n$ | 85 |
| **3** | 32.7(32.7) | 1.8(1.8) | 7.2(7.6) | – | 40.7(41.0) | $[UO_2L_3]_n$ | 72 |
| **4** | 42.9(43.0) | 2.2(2.2) | 9.1(9.4) | 7.8(8.0) | 16.9(15.6) | $[RuL_1 \cdot ClH_2O]_n$ | 68 |
| **5** | 43.0(43.0) | 2.3(2.4) | 9.8(10.0) | 8.6(8.5) | 17.8(18.1) | $[RuL_2ClH_2O]_n$ | 60 |
| **6** | 41.5(41.4) | 2.2(2.3) | 9.8(9.7) | 7.9(8.2) | 17.3(16.9) | $[RuL_3ClH_2O]_n$ | 55 |

*Microanalytical data as well as metal and chloride are in good agreement with the stoichiometry of the proposed complexes.
[a]The abbreviation $L_1$, $L_2$ and $L_3$ represent the deprotonated form of the ligands $L_1H_2$, $L_2H_2$ and $L_3H_2$. Insoluble in water and common organic solvents but soluble in coordinating solvents such as DMSO and DMF, colored, nonhygroscopic, air stable at room temperature for long periods.
[b]Estimated gravimetrically.



elemental analyses (table 1). The presence of coordinated water was confirmed by TGA where loss in weight corresponding to one and two water molecules occur at 180°C for $Ru^{3+}$ and $UO_2^{2+}$ complexes, respectively.

### 4.1. *Structure and stability*

It is known [10] that 8-hydroxyquinoline exists, in solution, in a monomer dimer equilibrium. The results of this study indicate that, in the monomeric form, a strong intramolecular hydrogen bond is present. This is in agreement with previous results [11]. Two such monomers lead to the dimer by forming additional hydrogen bonding yielding the bifurcated hydrogen bonds and H–N–H nitrogen bridges (scheme 1A).

In addition to the two bifurcated inter/intramolecular OH–N hydrogen bonds (scheme 1), two more intermolecular hydrogen bonding interactions are observed between nitrogen of azo/azomethine group and carboxylic/phenolic hydroxyl oxygen atom (scheme 2). This additional H-bonding does not influence the intramolecular distance, which shows a band at a lower frequency than the intermolecular interaction. This might be due to the additional H-bond which influences the hydrogen bonding ability of the carboxyl/hydroxyl group by electronic and/or steric factors. The overall structure of the dimer is close to planar with a slight shift of the two quinoline units from the plane. The dimer is able to dissociate, while the interamolecular interaction can only be broken if appropriate hydrogen bond acceptors are attached and act as competitors to the quinoline nitrogen atoms.

The two hydroxyquinoline units of the dimer (scheme 1D) are in one plane. The intermolecular **I** as well as intramolecular **II** hydrogen bonding occurs between the hydroxyl group and the quinoline nitrogen atom. The intermolecular hydrogen bond distance is shorter than the intramolecular one. This observation was also reported for other 8-hydroxyquinoline dimers and might be due to an unfavorable small O–H–N angle for the intramolecular interaction [9, 10].

Hydrogen bonding represents one of the most versatile interactions used for molecular recognition. Several attempts have been made to modulate the strengths of hydrogen bonds in synthetic host-guest systems [11] and in biological systems. In view

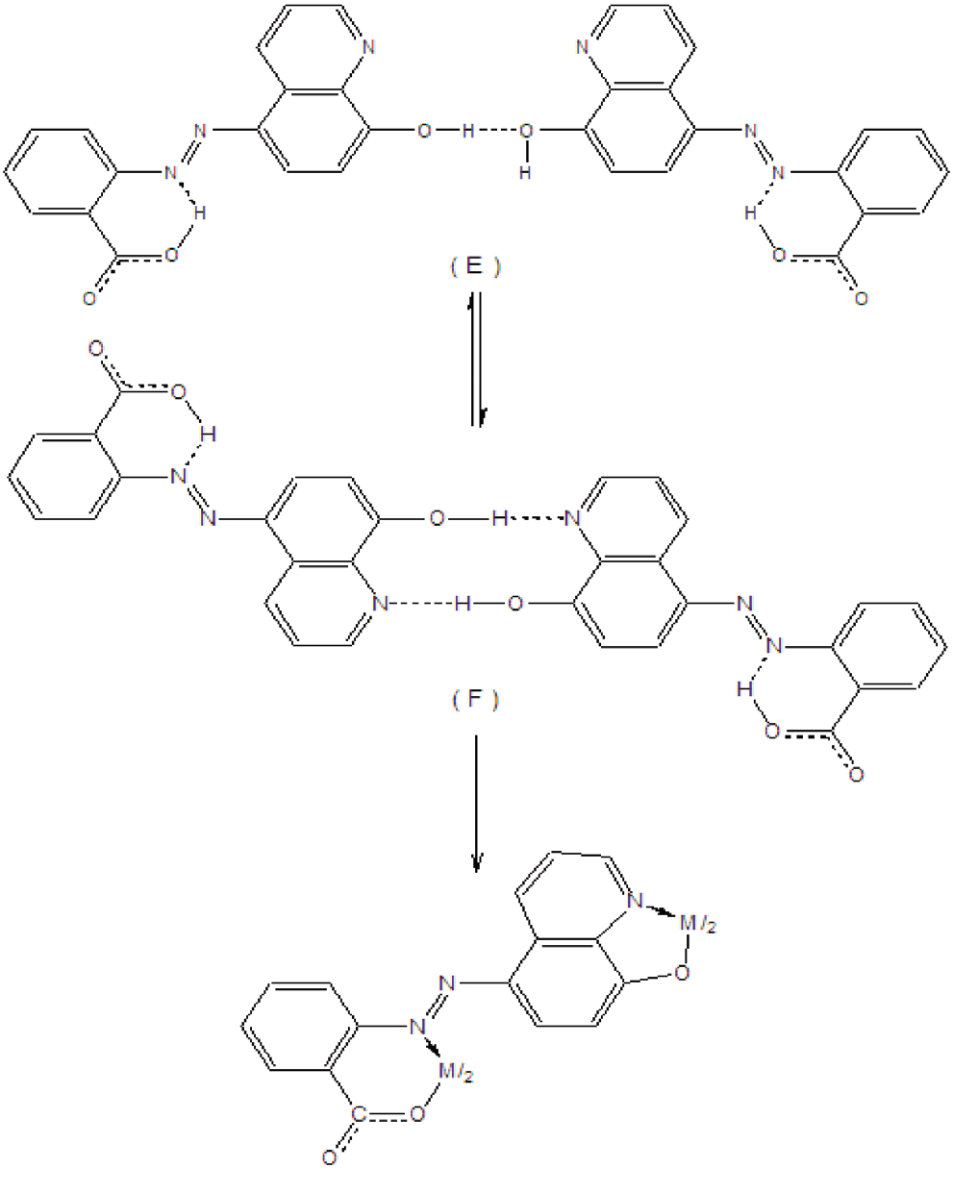


Scheme 2. General formula of 5-(2⁻-carboxyphenylazo)-8-quinolinol.

of the large differences in substituent effects (e.g., the Hammet-type substituent constants for –COOH and –OH); it might be possible to tune the strength of the hydrogen bond effectively by linking the hydrogen-bonding site to a reaction center through a conjugated spacer, and by altering the charge state of the reaction center. At the hydrogen-bonding end, azo/azomethine is used as a proton acceptor to form a hydrogen bond with COOH/OH of the ligand. The effects of protonation of COOH/OH on the strength of the hydrogen bond of the ligand are simulated as a function of the length of the $\pi$-conjugate.

An electron-withdrawing bridge would be expected to increase the acidity of the proton donor and hence increase its binding ability. The electron-withdrawing character of an azo group is relevant to signal-amplifying behavior [12]. The results indicate that in $LnH_2$ ($n = 1, 2$), the effects of the bridges are electron-withdrawing and electron-donating, respectively. Accordingly, the efficiency of $sp^2$-hybridized bridges is N=N > C=N.

The intra and intermolecular hydrogen bond in the carboxylic/phenolic hydroxyl hydrogen atom with N-atoms support the assignments suggested in the present work. The IR data of $L_1H_2$ shows a broad band accompanied with a noticeable decrease in wavenumber for the carbonyl stretching vibration of the carboxylic hydroxyl hydrogen group compared to stretching vibration of the phenolic hydroxyl hydrogen of $L_2H_2$. This supports the idea of intra and intermolecular hydrogen bonding. In fact, the band at $\sim 1685\,cm^{-1}$, assigned to the carbonyl group of the carboxylic free residue of $L_1H_2$ is shifted about $\sim 18\,cm^{-1}$ ($1667\,cm^{-1}$) in the complexes. This hydrogen bonding interaction will lead to: (i) rearranging the carboxylic group to the energetically more favorable *o*-coordination mode; (ii) stabilizing the chelate ring by intramolecular hydrogen bonding between oxygen hydrogen of this chelate ring and the basic nitrogen of the six-membered chelate ring (see schemes 1 and 2).

Infrared spectra of ligands show broad, medium intensity bands at ~3200–2800 ($L_1H_2$), 3450–2900 ($L_2H_2$), and 2180 and $830\,cm^{-1}$ due to the stretching frequency of the phenolic and carboxylic OH as well as the stretching vibration of hydrogen bonding. Detailed studies for different types of hydrogen bonds [3–6], have been carried out.

Intramolecular hydrogen bonds between the nitrogen atom of the –N = N– system and hydrogen of the carboxylic/phenolic hydroxyl hydrogen atom (six/five membered) and hydrogen ($C_8$–OH) and nitrogen of azomethine group (CNpy) are illustrated in scheme 1D. Intermolecular hydrogen bonding can form a cyclic dimer through the O–H–OH type between $C_8$–OH of one molecule and $C_8$–OH group of another (scheme 2E) and/or –N type between $C_8$–OH of one molecule and CNpy of another (schemes 1D and 2F).

In general, both COOH and OH groups are proton donors and their oxygen atoms are proton acceptors. Both intra and intermolecular OH–N may form a number of structures in a simultaneous equilibrium.

## 5. Electronic absorption spectra

The presence of an –OH group at the eighth position in the coupling moiety (figure 1) hinders the reaction, presumably, due to the hydrazone form [1] which destroys the planarity of the molecule in the azo form. This is expected to adversely affect the stability of the chelate structure.

$L_1H_2$ and polymer complexes in which the $C_8OH$ group is present show two absorption bands in the visible region at ~25,000 and ~21,740 ~20,840 $cm^{-1}$ due to azo-hydrazone tautomerism, which agrees well with similar systems [5, 13].

The lower wavelength band must be assigned to the $\pi$–$\pi^*$ transition of the azo form since all compounds in which the –OH group is methylated or complexed and thus, exist only in the azo form, have a single intense absorption at $\sim 25{,}000\,cm^{-1}$. The band at

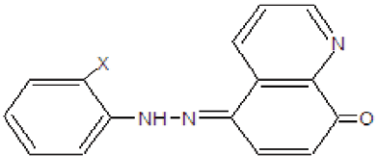


X = COOH ($L_1H_2$)
= OH ($L_2H_2$)
= SH ($L_3H_2$)

Figure 1. Representative structure of hydrazone form.

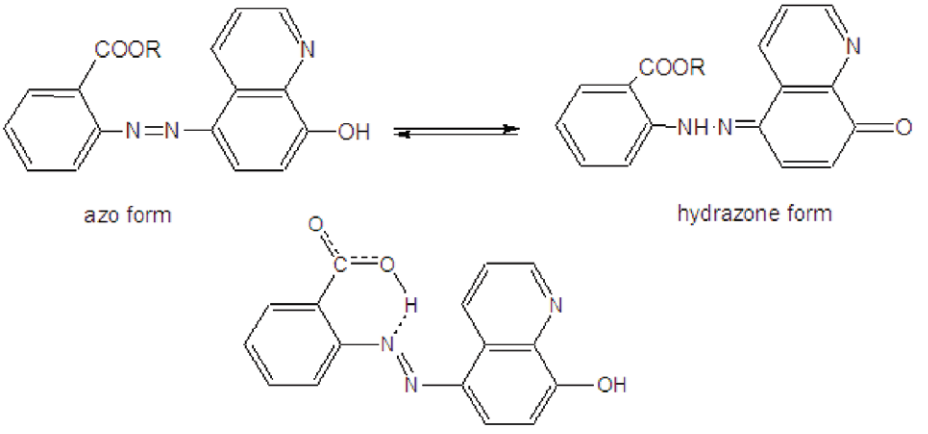


Figure 2. Representative structure of intramolecular H-bonding formed in the *o*-carboxylic compound.



~21,740–20,840 $cm^{-1}$ must, therefore, be attributed to the hydrazone form, which generally absorbs at a longer wavelength [14].

In an *o*-carboxylic compound, the existence of intramolecular H-bonding, as shown in figure 2, is possible. Estrification of the –COOH group is then expected to result in a large hypsochromic shift, consistent with intramolecular H-bonding. Such bonding is not favored in the corresponding hydrazone form.

Low energy absorptions of the complexes (28,000–17,000 $cm^{-1}$) result from the following: (a) transitions within the $UO_2^{2+}$ entity; and (b) equatorial ligand $\rightarrow UO_2^{2+}$ charge transfer. According to McGlynn [15] and Brint [16] the low energy region (28,000–17,000 $cm^{-1}$) is a T $\longrightarrow$ S process. McGlynn [15] and Gorller-Walrand [17] also stated that this absorption is due to excitation of an electron from a bonding orbital ($^1\pi_g$) of the $UO_2^{2+}$ entity to a non-bonding 5f–AO of uranium and it is virtually independent of the chemical nature of the equatorial ligands. It is known [17] that the total symmetry and equatorial coordination can exert some influence on this type of absorption spectra. Transitions of type **I**, scheme 1D are covered by a strong absorption corresponding to the $\pi \rightarrow$ f charge transfer from the equatorial ligand orbitals to the f-orbitals of the uranium atom and they are strongly affected by the chemical nature of

Table 2. $^1$H NMR spectral data ($\delta$ ppm)[b] of $LnH_2$ and its corresponding uranyl complexes.

| Compound[a] | OH (Phenolic and carboxylic) | Ar–H | HC=N |
|---|---|---|---|
| $L_1H_2$ | 8.82 | 6.78–8.40 | 8.94 |
| $[UO_2L_12H_2O]_n$[c] | – | 6.35–8.70 | 9.40 |
| $L_2H_2$ | 9.20 | 6.92–8.75 | 8.98 |
| $[UO_2L_22H_2O]_n$[c] | – | 6.35–8.70 | 9.25 |

[a]Solvent DMSO–$d_6$.
[b]Relative to TMS.
[c]A signal at 3.08 ppm is assignable to water.

the ligands within a given stereochemistry. The various bright colors of these complexes are ascribed to charge transfer bands [18].



## 6. $^1$H NMR spectra

$^1$H NMR spectra of $L_1H_2$ and $L_2H_2$ (table 2) show three singlets at $\delta$ 8.82 (2H), 9.2 (2H) and ~8.94 (1H) ppm due to the carboxylic-OH, phenolic –OH and azomethine HC=N groups, respectively. The aromatic and pyridine protons (11H) for ($L_1H_2$ and $L_2H_2$) appear as a number of complex multiplets in the regions between $\delta$ 6.78–8.40 and 6.92–8.75 ppm, respectively. The –OH proton signals exhibit fast exchange in the presence of $D_2O$, i.e., disappeared in presence of $D_2O$ consistent with the strongly hydrogen bonded in scheme 1. As reported in a previous study [19], hydrogen bonding leads to large deshielding of these protons. The shifts are in the sequence: O–COOH > O–OH. The $^1$H NMR spectra of diamagnetic complexes in DMSO–$d_6$ show a sharp singlet at about ~9.40 ppm (1H) due to the proton of the coordinated azomethine (CNpy) group, which is deshielded from its position in the free ligands. This is probably due to donation of the lone pair of electrons by the nitrogen to the central metal atom, resulting in the formation of a coordinate linkage [3] ($M \rightarrow N$). The aromatic and pyridine protons (11H) appear between $\delta$ 6.35–8.70 ppm.

## 7. $^{13}$CNMR

The $^{13}$C NMR of $L_1H_2$, $L_2H_2$ and their corresponding complexes **1** and **2** have also been recorded. These spectra provide direct information about the carbon skeleton of the molecules. Assignments of different resonances to respective carbon atoms are presented in figure 3 and table 3. A significant shift (table 3) in the positions of carbons attached to different participating groups clearly indicates the bonding of the nitrogen atom of pyridine and the oxygen atom of carboxylic and phenolic groups. Considering the non-equivalent pyridyl rings resulting from hydrogen-bonding, there are 13 unique carbon atoms in the molecules giving a total of 13 different peaks in the spectrum. In both pyridyl rings (figure 3a and b), the C(1) and C(7) carbon atoms adjacent to the more electronegative nitrogen and oxygen are shifted further downfield when compared

Table 3. $^{13}C$ NMR spectra (ppm) of $LnH_2$ and its corresponding uranyl complexes.

| Compound* | 1 | 2 | 3 | 4 | 5 | 6 | 7 | 8 | 9 | 10 | 11 | 12 | 13 | 14 |
|---|---|---|---|---|---|---|---|---|---|---|---|---|---|---|
| $L_1H_2$ | 156.22 | 117.90 | 182.20 | 123.35 | 142.80 | 126.08 | 131.24 | 152.20 | 138.30 | 119.30 | 115.90 | 129.00 | | 158.40 |
| 1 | 150.42 | 116.41 | 176.41 | 124.92 | 141.22 | 125.35 | 130.05 | 148.66 | 135.80 | 117.42 | 115.08 | 130.52 | | 154.00 |
| $L_2H_2$ | 157.20 | 118.00 | 182.00 | 122.90 | 143.08 | 126.82 | 132.08 | 152.05 | 138.55 | 119.81 | 115.80 | 129.00 | 159.05 | |
| 2 | 151.80 | 117.10 | 175.08 | 124.60 | 141.41 | 125.81 | 131.50 | 149.50 | 136.05 | 118.80 | 115.20 | 129.00 | 155.50 | |

*See table 1 anf figure 3.

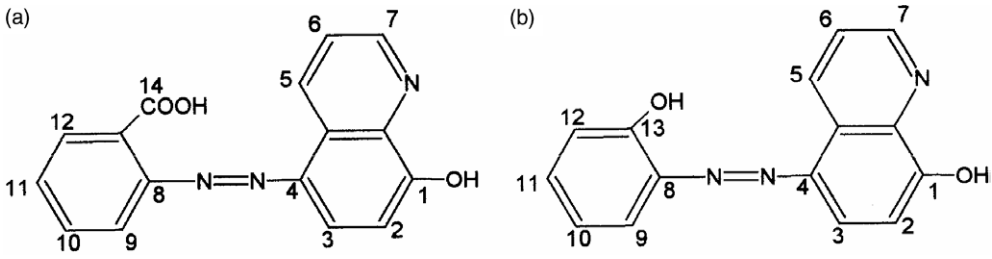


Figure 3. Representative structures of (a) $L_1H_2$ and (b) $L_2H_2$ ligands.

to the neighboring carbon atoms (table 4). This is also the case for the two carbon atoms C(8) situated ortho to the azodye. However, the non-protonated carbon atoms show more downfield shift in the pyridyl and/or phenyl rings due to an increase in electron density resulting from the presence of electronegative nitrogen and $\pi$-electron delocalization in the magnetic environment. The values in table 3 indicate clearly the differences in the $^{13}C$ chemical shifts for C(1), C(7), C(13) and/or C(14) before and after complex formation. Data for the free ligands $L_1H_2$ and $L_2H_2$ in DMSO–$d_6$ solution have been included for comparison. The different types of aromatic carbon in the substituted phenyl rings are distinguishable in the $^{13}C$ NMR spectra. The peak corresponding to C(14) (figure 3a) is observed upfield when compared to its counterpart C(13) in figure 3(b).



## 8. Bonding atoms and stereochemistry

### 8.1. *Geometry of dioxouranium(VI) polymer complexes*

The dioxouranium(VI) polymer, which is prepared from the ONO-donor, 5-(2$^-$-carboxyphenylazo)-8-quinolinol ($L_1H_2$) and 5-(2$^-$-hydroxyphenylazo)-8-quinolinol ($L_2H_2$), exhibits a $\nu$(O=U=O) vibrational mode at lower energy (916 and 923 $cm^{-1}$) than the dioxouranium(VI) polymer complex of the ONS-donor, 5-(2$^-$-thiophenylazo)-8-quinoliol ($L_3H_2$) ($\sim$932 $cm^{-1}$). Sulfur is expected to bind less strongly than oxygen to the hard Lewis acid, $UO_2^{2+}$ [20]. Moreover, the electron density at the uranium atom in ($L_1H_2$) and ($L_2H_2$) was greater than ($L_3H_2$) because oxygen is a harder Lewis acid than sulfur. An increase in electron density at uranium is expected to increase the repulsive force acting on the non-bonding electrons in the $UO_2^{2+}$ moiety, thus leading to weakening the U=O bond [21]. Since sulfur is more efficient than oxygen in electron delocalization, the electron density at uranium is reduced.

$\nu_3$-values of $UO_2^{2+}$ in ($cm^{-1}$) have been used to calculate the force constant ($F_{UO}$) in millidynes per angstrom (mdynes/Å) using McGlynn's method [22] and these ($F_{UO}$)-values on substitution in the Jones equation [23], $R_{UO} = 1.08\ (F_{UO})^{-1/3} + d$, yield the "UO" bond lengths in angstroms (table 4). The calculated $R_{U-O}$-values are in the range 1.72 to 1.75 Å in agreement with the range found from crystallographic measurements on various uranyl complexes [24]. Splitting of the $\nu_3$-band of $UO_2^{2+}$ in complexes **1**, **2** and **3**

Table 4. Variation of force constant (mdyn/Å), U–O bond distances (Å), frequencies ($cm^{-1}$), $\nu_1$ and $\nu_3$ of the isolated uranyl complexes.

| Complex[a] | $\nu_1$ | $\nu_3$ | $F_{UO}$ | $r_1$ | $r_2$ | $(F^s_{U-O})_t$ | $r_t$ | $(F^s_{U-O})_o$ | $r_o$ | $(F_{UO-UO^-})^b$ | $(\nu_1^2)^c$ | $F^*_{U-O}$ | $r_3$ | $(F_{UO-UO^-})^b$ | $(r_3-r_t)^2$ | $(r_1-r_t)^2$ | $(r_2-r_t)^2$ |
|---|---|---|---|---|---|---|---|---|---|---|---|---|---|---|---|---|---|
| **1** | 880 | 916 | 6.926 | 1.712 | 1.737 | 6.662 | 1.744 | 7.234 | 1.728 | −0.270 | 825.34 | 6.277 | 1.756 | −0.655 | $1.323 \times 10^{-4}$ | $1.050 \times 10^{-3}$ | $5.476 \times 10^{-5}$ |
| **2** | 885 | 923 | 7.032 | 1.706 | 1.734 | 6.465 | 1.750 | 7.316 | 1.726 | −0.286 | 826.47 | 6.338 | 1.754 | −0.700 | $1.44 \times 10^{-5}$ | $1.892 \times 10^{-3}$ | $2.592 \times 10^{-4}$ |
| **3** | 889 | 923 | 7.170 | 1.700 | 1.730 | 6.850 | 1.739 | 7.383 | 1.725 | −0.324 | 828.25 | 6.419 | 1.751 | −0.757 | $1.538 \times 10^{-4}$ | $1.529 \times 10^{-3}$ | $7.396 \times 10^{-5}$ |
| | | | | | | | | | | | | | | | $\sqrt{3.005 \times 10^{-4}}$ | $\sqrt{4.471 \times 10^{-3}}$ | $\sqrt{3.880 \times 10^{-4}}$ |
| | | | | | | | | | | | | | | | 0.01733 | 0.0669 | 0.0197 |

[a]The compex numbers correspond to that used in the table 1.
[1,2]Internuclear distance U–O calculated by using Badger equation and Jones equation.
$b_{U-O}$Force constant and UO–$UO^-$interaction constant with neglect the interaction of the UO bonds with the ligands, ($F_{UOUO}{}^-$bond–bond interactions).
[c]Symmetric stretching frequencies evaluated by using El-Sonbati equation.
$(F^s_{U-O})_t$ Is the true value of force constant.
$(F^s_{U-O})_a$ Is the constant calculated with neglect of the ligands.
$F^s_{U-O}$ Is the bond force constant which evaluated by using El-Sonbati equation.
[$r_t$]Internuclear distance U–O calculated by using the value of force constant.
[$r_a$]Internuclear distance U–O calculated by using the asymmetric stretching frequency with neglect of the ligands.
[$r_3$]Internuclear distance U–O calculated by using the symmetric stretching frequency evaluated buy using El-Sonbati equation.

may be due to stacking disorder or unit cell coupling [24]. $\nu_3$-Values of $UO_2^{2+}$ decrease when the donor properties are strengthened or when the number of donor ligands in the equatorial plane is increased and thus the stability of uranyl complexes should increase [22]. The experimental results reveal an excellent linear relation between $\nu_1$ and $\nu_3$ with the slope corresponding to $(1+2M_O/M_U)^{1/2}$; where $M_O$ and $M_U$ are the masses of oxygen and uranium atoms, respectively. Instead of the linearity between $\nu_1$ and $\nu_3$ frequencies, the El-Sonbati equation [25] has focused attention on their normalized differences, which do not depend on the masses of oxygen and/or uranium atoms.

The force constant deduced from the spectral data used herein for the U–O bond [$F_{U-O}$ mdyn/Å], $(F^s_{U-O})_t$, $(F^s_{U-O})_o$ and $F_{OU,OU^-}$; with neglect to the interaction of the U–O bonds with the ligands, and the U–O bond distance [$r_{U-O}$ Å] are presented in (table 4).

Perhaps new light can be shed on the problem by looking at the values of $r_1$, $r_2$ and $r_3$ from a different point of view. It might be worthwhile to focus attention on their normalized differences. Thus a new relationship between them with respect to $r_t$ (table 4) was determined by Global error which shows excellent validity in the sequence: $\sqrt{(r_3-r_t)^2} > \sqrt{(r_2-r_t)^2} > \sqrt{(r_1-r_t)^2}$.



### 8.2. *Geometry of ruthenium(III) complexes*

**8.2.1. Magnetic moments and electronic spectra.** The magnetic susceptibility measurements at room temperature show that the magnetic moments of ruthenium complexes lie in the range 1.7–2.1 BM (table 5) corresponding to one unpaired electron.

The electronic spectra of ruthenium(III) azoquinoline complexes under study show three groups of bands. The absorption bands seem always to be of the same pattern through appearing with varied extinctions and changed absorption maxima which can be ascribed to changes in the molecular structure of the ligands leading to varied strength in the azoquinoline $\rightarrow Ru^{3+}$ interaction. Of the three regions, the bands with frequencies above 34,000 $cm^{-1}$ can be assigned to localized $\pi \rightarrow \pi^*$ transitions of the aromatic system. The bands within the 20,000–34,000 $cm^{-1}$ region represent various

Table 5. Electronic spectra and ligand field parameters ($cm^{-1}$) for octahedral ruthenium(III) complexes (for compositions see table 1).

| Complex[a] | Bands(obs.) ($cm^{-1}$) | $\mu^{bc}_{eff}$(B.M.) | $\nu_2/\nu_1$ | 10Dq | $B$ | $\beta$ | C | $F_2^d$ | $F_4^d$ | $Z^*$ |
|---|---|---|---|---|---|---|---|---|---|---|
| **4** | 13650<br>17000<br>19430 | 1.76 | 1.25 | 21356 | 423 | 0.72 | 1645 | 658 | 47 | 0.77 |
| **5** | 13480<br>16950<br>18530 | 1.79 | 1.26 | 22121 | 436 | 0.76 | 1715 | 681 | 49 | 0.84 |
| **6** | 14385<br>17980<br>19700 | 2.1 | 1.25 | 22918 | 453 | 0.81 | 1785 | 708 | 51 | 0.92 |

[a]See note a in table 1.
[b]Per metal.
[c]Measured at room temperature.
[d]Condon-Shortly parameters.

types of CT interactions either within the ligand molecule (interaligand CT) or due to $L \rightarrow Ru^{3+}$ or $Ru^{3+} \rightarrow L$ CT interactions. The third group of bands lying below 20,000 $cm^{-1}$ usually exhibits three distinct peaks. These can be attributed to three spin forbidden d–d transitions at ~13,350–14,400 ($^2T_{2g} \rightarrow {}^4T_{1g}$), 16,950–18,200 ($^2T_{2g} \rightarrow {}^4T_{2g}$) and 19,250–19,800 $cm^{-1}$ ($^2T_{2g} \rightarrow {}^2A_{2g}$, $^2T_{1g}$) as expected for octahedral symmetry of low spin $Ru^{3+}$ complexes [3]. The electronic spectra of these complexes are further rationalized in terms of ligand field parameters and interelectronic repulsion parameters by using known equations [26] (neglecting the configurational interaction). The values of these parameters, given in (table 5), are comparable to those reported for other ruthenium(III) derivatives involving nitrogen and oxygen donor molecules [3].

The lower values of the Racah interelectronic repulsion parameter B in comparison to the free ion value indicate strong covalent bonds occuring between the ligands and the central metal ion. Greater reduction in B indicates greater covalency in the metal-ligand bond and smaller effective charge experienced by the d-electrons [26]. The overall effect will be an increase in the observed Dq value; high Dq values are usually associated with considerable electron delocalization [27]. Decreasing values of the nephelauxetic ratio $\beta$ are also associated with a reduction in the effective positive charge of the metal ion and with an increasing tendency to reduction to the next lower oxidation state. For 4d transition metals, variations of the Racah interlectronic repulsion parameter with the cationic charge $Z^*$ and the number (q) of electrons in the partially filled d-shell is expressed by the relation [28].

$$B(\mathrm{cm}^{-1}) = 472 + 28q + 50(Z^* + 1) - \frac{500}{Z^* + 1}$$

This gives effective ionic charges of the ruthenium(III) azoquinoline complexes in the 0.77–0.92 range, which are considerably below the formal +3 oxidation state of the metal ion. It is apparent that the nephelauxetic ratio $\beta$ depends greatly upon the electronegativity of the donor atoms and the ligand structure.

As can be seen from table 5, the Racah parameters $B$, $\beta$, and $\mu_{eff}$ values $F_n$, $Dq$ and $Z^*$ values increase from compound **4** to **6**. This can be attributed to the fact that the effective charge experienced by the d-electrons decreases due to the electron withdrawing in $L_1H_2$ while it increases by the electrons donating charater in $L_2H_2$ and $L_3H_2$.

## 9. Thermal analysis of uranium and ruthenium

The DTA data of complexes (**1–6** except **3**) exhibited lose of weight in three steps from 75 to ~170°C, ~185 to ~270°C and from ~310 to ~590°C. The coordinated water molecules in all complexes (except complex **3**) are removed at temperature around ~180°C, indicated by an endothermic peak with maximum at 180°C. This is followed by removal of coordinated Cl (in complexes **4–6**) within the temperature range 185–280°C. Four exothermic peaks with maxima at 290, 370, 450 and 580°C would indicate a series of rearrangements followed by oxidative degradation of the

intermediate complexes formed by partial loss of organic species and finally phase transformation of metal oxides [3, 6].

## 10. Stereochemistry and mode of bonding of the complexes

IR spectroscopy is known to be a powerful tool for structural determinations of the ligands and metal chelates. The assignments of fundamental functional groups are basic for such purposes.

A partial assignment of the absorption bands for $LnH_2$ (scheme 1B), shows four potential donor sites: (i) COOH, OH, SH; (ii) azo nitrogen atom; (iii) $C_8$–OH and (iv) nitrogen pyridine (CNpy). Due to the 1, 2-position of these donor groups in the molecule, six- and/or five-membered chelate ring formation is possible on complexation.

The –OH stretching frequency and intensity of phenol derivatives depends on many factors (e.g., constituents, medium, etc.). Hoyer [29] reviewed the relationship between the hydrogen bond band and the –OH stretching frequency. In addition, many other researchers examined the problem in finer and more quantitative data [3–6, 11, 29]. Thus IR data are important to explain and justify the bonding in this study.



All of the free ligands show characteristic CN (1555), –N = N–(1540) and OH ($3200\,cm^{-1}$) frequencies. The CN and N–N bands shift towards lower frequency in the spectra of the complexes due to involvement of the N atom, whereas the $\nu$(OH) bands almost disappear due to the deprotonation of the OH group. A strong band at $\sim 1685\,cm^{-1}$ in $L_1H_2$ is assigned to the carbonyl stretch of the carboxylic group [5]. Ionization of carboxylic group results in an equilibrium resonance of the two C–O bonds of the carboxylate group (schemes 1 and 2) and disappearance of the characteristic carbonyl absorption. Two new bands are expected in the ranges $1605–1540\,cm^{-1}$ corresponding to the asymmetric and symmetric vibrations of the $COO^-$ structure [16]. In the metal complexes of $L_1H_2$, the strong carbonyl band disappears and is replaced by a strong broad absorption at $1350\,cm^{-1}$, which is assigned to the symmetrical vibration of the carboxylate group [17].

The absence of the O–H absorption bands and the replacement of the C=O vibration by a band assigned to the resonated carboxylate group in the spectra of the metal complexes is indicative of metal attachment to the anionic ligand via the carboxylate oxygen atom. Also, the disappearance in the spectra of all the complexes of a broad band ($\sim 3440\,cm^{-1}$)($L_2H_2$) $\nu$(OH) vibration, and a weak band ($\sim 2575\,cm^{-1}$)($L_3H_2$)$\nu$(SH) indicate deprotonation of phenolic and thiolic protons on complexation. The participation of phenolic oxygen and thiolic sulphur in coordination to the metal is further supported by an upward shift in $\nu$(C–O)($\sim 1340\,cm^{-1}$) to the extent of $8–10\,cm^{-1}$ and a downward shift in $\nu$(C–S)($\sim 760\,cm^{-1}$) by $10–15\,cm^{-1}$ in all complexes. The $\nu$(C–N) vibration at $\sim 1490\,cm^{-1}$ in the ligand suffers a downward shift of $\sim 8\,cm^{-1}$ upon complexation, thereby supporting the coordination of one of the azo nitrogen atoms to the metal ion. The presence of coordinated water in all complexes except complex **3** is indicated by a sharp band at $\sim 3445\,cm^{-1}$ and two somewhat weaker bands at $\sim 845$ and $690\,cm^{-1}$, which could be assigned to OH stretching, rocking and wagging vibrations, respectively [3]. The appearance of some new bands in the IR spectra of the metal complexes are probably due to the formation of M–O, M–N and M–S bonds through complexation [18, 19].

## 11. Conclusion

The results arising from the present investigations confirm that hydroxyquinoline exists, in solution, in a monomer/dimer equilibrium. The results suggest that in the monomeric form a strong intramolecular hydrogen bond is present. Two monomers lead to the dimer by formation of additional hydrogen bonds yielding the bifurcated hydrogen bonds and H–N–H nitrogen bridges (scheme 1A). The dimer dissociates, if the intramolecular interaction can be broken by hydrogen bond acceptors to act as competitors to the quinoline nitrogen atoms (scheme 1D). At the hydrogen bonding end, azo/azomethine is used as a proton acceptor to form a hydrogen bond with COOH/OH of the ligand. Protonation of the COOH/OH on the strength of the hydrogen bond of the ligand is simulated as a function of the length of the $\pi$-conjugation. The strong chelating ability of $LnH_2$, which contains the –N=C group, is considered to result, in part, from the d$\pi$–p$\pi$ bonding from the metal to the ligand; this $\pi$-bonding imparts some aromatic character to the chelate ring. The above results show clearly the effect of substitution in the ortho position of the benzene ring on the stereochemistry of both $Ru^{3+}$ and/or $UO_2^{2+}$ complexes. The results also suggest that the existence of a hydroxyl and/or thiolic group enhances the electron density on the coordination sites and simultaneously increases the values of Racah parameters of $Ru^{3+}$ complexes. The low molar conductance values of all the complexes indicate their non-ionic character. The complexes decomposed on heating at >300°C and were almost insoluble in water. TGA confirmed the presence of coordinated water, where loss in weight corresponding to one water molecule for $Ru^{3+}$ and two coordinated water molecules of the uranyl complexes (except complex 3) occur at 180°C.

In conclusion, the results of the present study indicate that the selected 5-(2$^-$-alkyl phenylazo)-8-quinolinol ($LnH_2$) ligands are suitable for building a supramolecular structure. Furthermore, the azo and/or hydrazo compounds are known to experience photochemical isomerization [30] and are, therefore, of interest for applications. The polymeric complexes of $Ru^{3+}$ and $UO_2^{2+}$ with 5-(2$^-$-alkyl phenylazo)-8-quinolinols ($LnH_2$) may be considered as promising supramolecules, which could be useful in molecular materials.



## References

[1] S. Patal. *The Chemistry of Hydrazo, Azo, and Azoxy Groups*, Part 1, Wiley, New York (1975).
[2] D.A. Pearce, N. Jotter, I.S. Carrico. *J. Am. Chem. Soc.*, **123**, 3224 (2001).
[3] A.T. Mubarak, S.A. El-Assiery. *Appl. Organomet. Chem.*, **18**, 343 (2004).
[4] A.T. Mubarak. *Desig. Mon. and Polym.*, **8**, 1 (2005).
[5] A.Z. El-Sonbati, A.A. Belal, S.I. El-Wakel, M.A. Hussien. *Spectrochim. Acta Part A*, **60**, 965 (2004).
[6] A.T. Mubarak. *Spectrochim. Acta Part A*, **61**, 1163 (2005).
[7] G. Ebert. *Biopolymer; Tenbner; Stuttgart*, **23**, 6 (1993).
[8] W.I. Jørgensen, J. Pranata. *J. Am. Chem. Soc.*, **112**, 2008 (1990).
[9] M. Albrecht, K. Witt, E. Wegelins, K. Rissanen. *Tetrahedron*, **56**, 591 (2000).
[10] M. Albrecht, O. Blau, E. Wegelins, K. Rissanen. *New J. Chem.*, **23**, 667 (1999).
[11] G. Cook, V.M. Rotello. *Chem. Soc. Rev.*, **31**, 275 (2002).
[12] A. Niemz, V.M. Rottello. *Acc. Chem. Res.*, **32**, 44 (1999).
[13] H. Suzuki. *Electronic Absorption Spectra, and Geometry of Organic Molecules*, Academic Press, New York (1967).
[14] J. Griffithr. *Colour and Constitution of Organic Molecules*, Academic Press, New York (1976).
[15] S.P. McGlynn, J.K. Smith. *Mol. Spectro.*, **6**, 164 (1973).

[16] P. Brint, A.J. McCaffery. *Mol. Phys.*, **25**, 311 (1972).
[17] C. Gorller-Walrand, S.D.E. Jeogere. *Spectrochim. Acta*, **28A**, 257 (1972).
[18] A.T. Mubarak, A.Z. El-Sonbati, A.A. El-Bindary. *Appl. Organomet. Chem.*, **18**, 212 (2004).
[19] A.Z. El-Sonbati, A. El-Dissouky, A.A. El-Bindary, A.S. Hilali. *Spectrochim. Acta Part A*, **57**, 1163 (2001).
[20] R.G. Pearson. *J. Am. Chem. Soc.*, **83**, 3333 (1963).
[21] J.P. Doy, L.M. Venanzi. *J. Chem. Soc. (A)*, 1363 (1966).
[22] S.P. McGlynn, J.K. Smith, W.C. Nelly. *J. Chem. Phys.*, **35**, 105 (1961).
[23] L.H. Jones. *Spectrochim. Acta*, **10**, 395 (1958), 11, 409 (1959).
[24] J.I. Bullock. *J. Chem. Soc. (A)*, 781 (1969).
[25] A.Z. El-Sonbati. *Spectrosc. Lett.*, **30**, 459 (1997).
[26] A.B.P. Lever. *Inorganic Electronic Spectroscopy*, 2nd Edn, Elsevier, Amsterdam (1984).
[27] B.N. Figgis. *Introduction to Ligand Fields*, Wiley Eastern, New Delhi (1976).
[28] C.K. Jorgensen. *Helv. Chem. Acta*, **56**, 131 (1967).
[29] H. Hoyer. *Z. Electrochem.*, **49**, 97 (1943).
[30] Z. Sekka, C.S. Kang, E.F. Aust, G. Wegner, W. Knoll. *Chem. Mater.*, **7**, 142 (1995).